Computational and experimental evaluation on pyrazoles as corrosion inhibitor in HCl solution: DFT and electrochemical analysis

R.K. Mitra,[1] R. Yadav,[2] A. Tomar[2] and M. Yadav[1]*

[1]*Department of Chemistry and Chemical Biology, Indian Institute of Technology (ISM), Dhanbad 826004, India*
[2]*Department of Computer Science and Engineering, Noida International University, Greater Noida, UP, India*
**E-mail: mahendra@iitism.ac.in*

Abstract

Traditionally for the selection of effective corrosion inhibitors, various organic compounds are synthesized and their corrosion protective ability is measured but out of large number of tested compounds only few are found efficient which results in time loss, chemical loss and finally money loss. To overcome these problems computational analysis is executed on compounds. For this, initially compounds are analyzed by density functional theory (DFT) calculations and if favorable results are found then only those compounds are synthesized for corrosion inhibition studies. Thus, application of computational analysis has paved the way for the cost-effective identification of efficient corrosion inhibitors. In this study corrosion preventing ability of pyrazoles, namely, 2-(3,5-bis(4-methoxyphenyl)-4,5-dihydro-1*H*-pyrazol-1-yl)-4-phenylthiazole (BMPP) and 2-(3,5-bis(4-chlorophenyl)-4,5-dihydro-1*H*-pyrazol-1-yl)-4-phenylthiazole (BCPP) was studied on N80 steel (NS) in 15% HCl solution using DFT, gravimetric and electrochemical methods. The compounds BMPP and BCPP offered corrosion protection ability of 97.98 and 94.95%, respectively, at 500 ppm concentration towards NS facet through mixed adsorption by obeying Langmuir isotherm. Both compounds exhibited mixed inhibitor nature. The computational predictions about corrosion inhibition behavior of both compounds were in agreement with experimental observations. The results of surface analysis performed by FE-SEM, AFM and XPS suggested the fabrication of inhibitor corrosion protective film at the NS facet.

Received: June 7, 2024 Published: September 30, 2024 doi: 10.17675/2305-6894-2024-13-4-2

Keywords: *DFT, electrochemical study, pyrazoles, corrosion inhibitor, N80 steel.*

1. Introduction

Ever since the early industrial revolutions, corrosion has been acknowledged as a significant social issue. The expense of corrosion emitted by industries has steadily risen over time and the damage by corrosion to materials is directly correlated to productivity. In 2016, the NACE (National Association of Corrosion Engineers) International released a

testimony stating that 3.4% of the GDP of world, or 2.5 trillion USD, is attributed to corrosion. The petroleum industry is among the most severely impacted, as leaks and oil spills not only contribute significantly to production costs but also negatively impact surrounding natural resources. Many times, corrosion also becomes cause of fatalities as well as industrial shutdown [1–3]. N80 steel (NS) is the main constructional material widely used in transmission pipelines, down-hole tubular, casings, and flow lines across the petroleum industries. During crude oil-well acidization, 15% to 28% hydrochloric acid solution is prevalently passed through N80 steel tubing to open oil bores and to remove deposits of silicates and carbonates in crude mining processes. This process is called acidizing which is prevalently utilized to increase oil production [4–7]. The acidizing process greatly corrodes the N80 steel used in fabrication of casing and tubing. Hence, corrosion inhibitors (C.I) are added to the acid solution while performing the acidizing process [8, 9]. Utilization of C.I is the most practical and affordable method to defer attack by corrosion on metals. The affordability, inhibition efficiency, and its environmental impact, play a major role in selection of an efficient inhibitor. The efficiency of corrosion inhibitor mainly depends on type of interaction of inhibitor with the metallic material. Inhibitors show interaction of charge with the metal substrate called as physisorption or chemical interaction called as chemisorption by undergoing involvement of electron share with metal facet. However, C.Is usually exhibit a combination of chemisorption and physisorption phenomenon simultaneously, referred to as mixed adsorption. The C.Is illustrating the dominant physisorption phenomenon demonstrate lowering of efficiency with temperature rise as a result of breaking of the formed inhibitive layer on metal. Whereas, C.Is displaying dominant chemisorption mechanism, tend to achieve nearly constant inhibition efficiency on going to elevated temperatures. Effectiveness of inhibitors also depends on the stability of adsorbed passive layer on substrate [10–13].

The majority of the documented organic inhibitors work as less toxic and effective C.I. Therefore, it's important to look for novel organic C.I which is safe and effective for NS in acidic solution. It is documented in literature that various organic heterocyclic compounds consisting of nitrogen, sulfur and oxygen work as efficient corrosion inhibitor for steel in acidic environment [14–17]. Pyrazole is a heterocyclic five-member compound consisting of three carbon atoms and two nitrogen atoms in the *ortho* positions. Due to the presence of nitrogen atoms and pi- electrons, pyrazole compounds easily adsorbed at the metal surface and facilitate the corrosion inhibition process. Pyrazole derivatives offer variety of biological activities such as anti-inflammatory, antimicrobial, antifungal, antihyperglycemic, antitumor and pesticidal. In addition to these biological activities, pyrazole compounds have been documented in literature as good corrosion inhibitor in acidic environments [18–26].

Citing the good corrosion inhibition efficiency of pyrazole derivatives and significance of C.Is in industrial applications, this work focused on the synthesis and utilization of BMPP and BCPP as corrosion inhibitor for NS in acidic solution.

2. Experimental Procedures

2.1. N80 steel samples preparation

N80 steel samples bearing sizes 30×20×1 mm were employed for weight loss analysis whereas working electrode of 1 cm^2 bare area was utilized for electrochemical testing. N80 steel samples with composition (*wt.*%): C = 0.31; Cr = 0.20; Si = 0.19; P = 0.010; Mn = 0.92; S = 0.008 and remaining Fe were utilized for the corrosion test. Before initiating the test, NS samples were finely polished (with 80, 150, 360, 400, 600, 1000, 1200 and 2000 grades emery papers), cleaned with water, acetone and dried.

2.2. Preparation of 15% HCl solution

Sigma Aldrich 37% HCl was purchased and utilized for the preparation of 15% HCl solution by dilution with double distilled water. Both C.Is (BMPP and BCPP) different concentrations (100–500 ppm) were prepared in 15% HCl solution. Volume of the testing solution was 250 mL and 150 mL for gravimetric analysis and electrochemical analysis, respectively.

2.3. Synthesis of BMPP and BCPP

Synthesis of inhibitors, BMPP and BCPP was done by adopting the procedures outlined in the literature [27, 28] as shown in Scheme 1. The compounds 1-thiocarbamoyl-3,5-diaryl-2-pyrazoline derivatives (b) were prepared by refluxing the mixture of 1,3-diaryl-2-propen-1-ones (chalcones) (a) and thiosemicarbazide in ethanol for 24 h and maintaining the alkaline pH by drop wise regular addition of NaOH. The compounds 2-(3,5-bis(4-methoxyphenyl)-4,5-dihydro-1*H*-pyrazol-1-yl)-4-phenylthiazole [BMPP] and 2-(3,5-bis(4-chlorophenyl)-4,5-dihydro-1*H*-pyrazol-1-yl)-4-phenylthiazole [BCPP] were prepared by refluxing compound (b) with phenacetylbromide in ethanol. The structure of BMPP and BCPP is shown in Figure 1. Both the compounds were characterized.

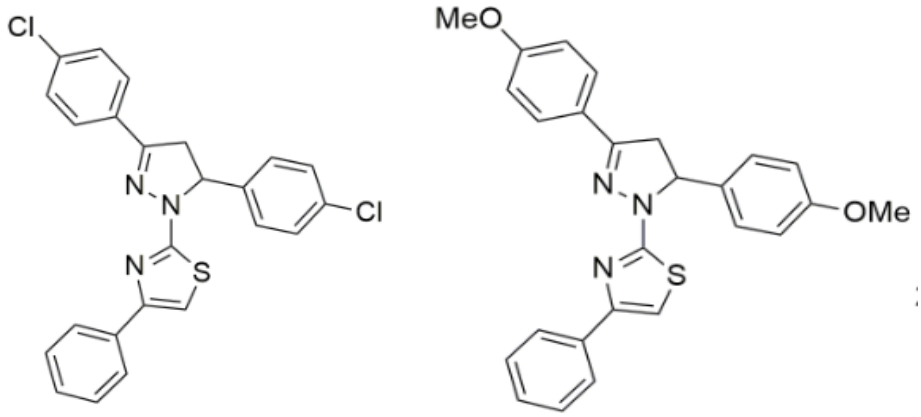

[BMPP] [BCPP]

Figure 1. Structures of BMPP and BCPP.

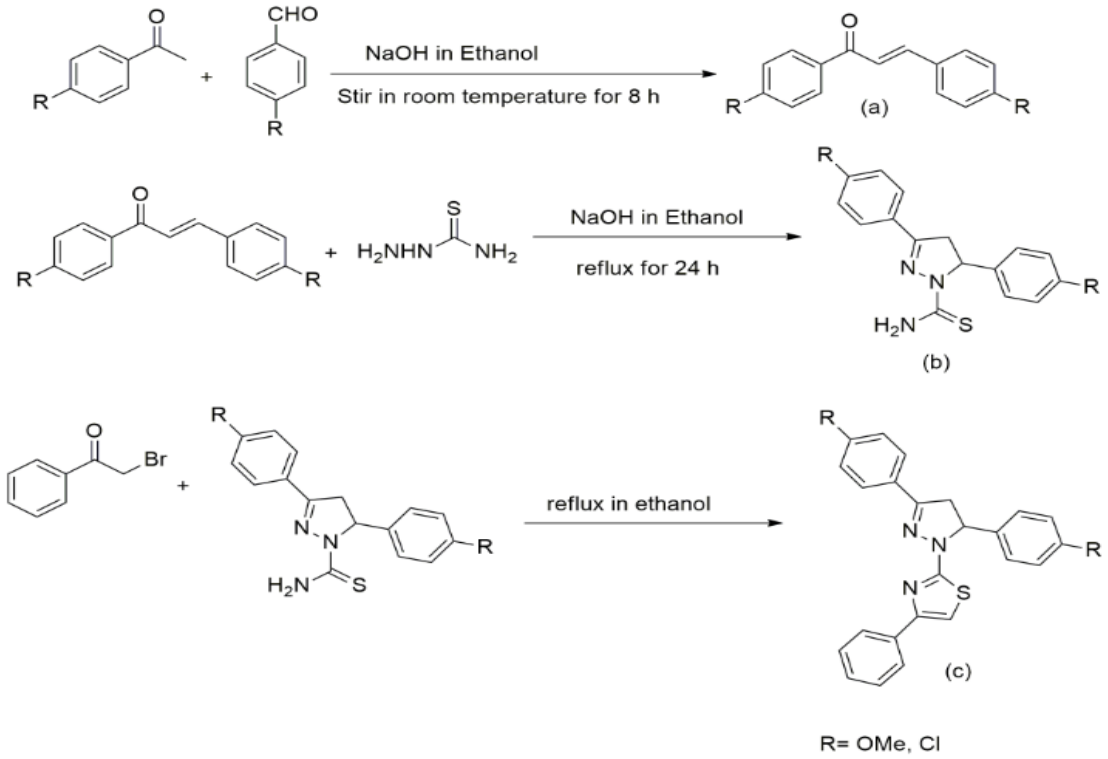

Scheme 1. Synthetic route of BMPP and BCPP.

BMPP

Yield 87%; Analytical data calculated for $C_{26}H_{23}N_3SO_2$, elements (%) theoretical/ observed: C (70.75/70.64); H (5.22/5.21); N (9.52/9.49), S (7.26/7.25). FTIR (KBr) (cm^{-1}); 3030 (Ar–C–H), 1610 (C=N), 1060 (C–O), 710 (C–S).

BCPP

Yield 88%; Analytical data calculated for $C_{24}H_{17}N_3O_2SCl_2$, elements (%) theoretical/ observed: C (64.14/64.18); H (3.79/3.81); N (9.35/9.32), S (7.13/7.16). FTIR(KBr) (cm^{-1}); 3020 (Ar–C–H), 1620 (C=N), 1060 (C–O), 720 (C–S).

2.4. Gravimetric analysis

This analysis was carried out following the ASTM G-31 standards for corrosion testing and measurements [29]. The polished N80 steel samples were precisely weighed and recorded. Analysis was carried out in triplicate basis to ensure accuracy in measurements. Samples were immersed for 6 h in 250 mL of 15% HCl solution for each concentration starting from blank 15% HCl (0 ppm) at different temperatures. Analysis was done at temperatures, 303, 313, 323 and 333 K. After 6 h, specimens were taken out from solution and the corrosion product formed on the N80 steel samples was removed, washed with double distilled water followed by acetone and finally dried, before recording the final

weight loss readings. Average of the triplicate readings was taken for calculating the final corrosion rate.

Following equations were used to calculate corrosion rate (*CR*), inhibition efficiency (%η) and surface coverage area (θ).

$$CR = \frac{\left(8.76 \cdot 10^4 \cdot \Delta W\right)}{A \cdot T \cdot D} \tag{1}$$

$$\%\eta = \frac{\left(CR_0 - CR_i\right)}{CR_0} \cdot 100 \tag{2}$$

$$\theta = \frac{\%\eta}{100} \tag{3}$$

Here, *CR*, *A*, Δ*W*, *T* and *D* are NS sample corrosion rate (mm y^{-1}), exposed area (cm^2), weight loss (mg), exposure period (h) and density of N80 steel ($g \cdot cm^{-3}$), respectively. CR_0 is the corrosion rate in the absence of an inhibitor and CR_i is the corrosion rate in the presence of an inhibitor, respectively.

2.5. Electrochemical studies

For electrochemical studies, corrosion cell consisting of N80 steel of 1 cm^2 bare surface area, SCE and Pt as working, reference and counter electrode was used. The stability of electrochemical setup was verified by conducting OCP (open circuit potential) test. After attaining stable OCP, the EIS testing was performed in the frequency range 100 kHz to 1 Hz with an AC amplitude of 10 mV. In EIS, Nyquist and Bode plots were recorded concurrently. The potentiodynamic polarization (PDP) study was done in the ±2.5 V potential and 0.5 mV/s scan rate. Tafel parameters like β_a (anodic slope), β_c (cathodic slope), E_{corr} (corrosion potential) and i_{corr} (corrosion current density) were measured [30]. Experiments were performed on a Corrtest potentiostat/galvanostat/electrochemical workstation Model: CS350, equipped with CS studio 5 software.

2.6. FESEM and AFM analysis

For FESEM and AFM analysis of samples, FESEM instrument made by Carl Zeiss, Germany, model: Supra 55 and AFM instrument made by Bruker Corporation (Multi-Mode 8and Dimension Icon) was utilized to know about the changes occurring at NS facet as a result of corrosion.

2.7. XPS analysis

XPS of samples after the corrosion prevention was done utilizing the PHI III scanning XPS equipment. In XPS spectra binding energy associated with C_{1S}, N_{1S}, O_{1S}, and Fe_{2P} was determined.

2.8. Computational study

DFT (Density Functional Theory) calculations were done utilizing the Gaussian-09 program [31]. The geometry of the inhibitors was optimized in the gas phase and aqueous phase using the first exchange correctional, hybrid B3LYP functional, using 6-31 G (d, p) basis sets. [32]. The Gauss View 5.0 software was employed to envisage the frontier molecular orbital [33].

3. Results and Discussion

3.1. Gravimetric study

Gravimetric study was done to evaluate the corrosion protection efficiency of inhibitors BMPP and BCPP for N80 steel in 15% HCl solution. Effect of increase in concentration and temperature on the corrosion rate and protection efficiency of the inhibitors was evaluated quantitatively and reported in Table 1. It can be seen from the Table 1 that for the inhibitors BMPP and BCPP, on increasing the concentration of inhibitor in test solution, %η (inhibition efficiency) is increasing, but on increasing temperature, decline in %η is seen, which led to conclude that physisorption type of interaction is dominantly occurring between the inhibitors and N80 steel. Maximum inhibition efficiency achieved by the inhibitor BMPP is 97.98% at 500 ppm at 303 K and BCPP is 94.95% at 500 ppm at 303 K. Hence, we can say that inhibitor BMPP is comparatively more efficient than inhibitor BCPP. When concentration of inhibitors BMPP and BCPP in the test solution is increased, more number of corrosive species like H_2O or Cl are displaced from the N80 steel surface and more adsorption of inhibitor molecules on N80 steel surface occurred, creating an inhibitive film between the N80 steel and the acid solution, hence preventing corrosion.

Table 1. Gravimetric measurements for N80 steel in 15% HCl solution in the absence and presence of inhibitors BMPP and BCPP at 303–333 K.

Temp.	**303 K**			**313 K**			**323 K**			**333 K**		
Conc., ppm	***CR*, mm y^{-1}**	**θ**	**η%**	***CR*, mm y^{-1}**	**θ**	**η%**	***CR*, mm y^{-1}**	**θ**	**η%**	***CR*, mm y^{-1}**	**θ**	**η%**
Blank	20.20	–	–	34.55	–	–	55.47	–	–	92.69	–	–
						BMPP						
100	4.96	0.75	75.41	8.87	0.74	74.31	16.02	0.71	71.11	30.02	0.68	67.61
200	2.89	0.86	85.66	5.50	0.84	84.06	10.17	0.82	81.66	20.06	0.78	78.36
300	1.77	0.91	91.23	3.37	0.90	90.23	6.58	0.88	88.13	13.69	0.85	85.23
400	1.01	0.95	95.21	2.17	0.94	93.71	4.77	0.91	91.40	10.75	0.88	88.40
500	0.406	0.98	97.98	1.71	0.95	95.03	3.92	0.93	92.93	9.24	0.90	90.03

Temp.	**303 K**			**313 K**			**323 K**			**333 K**		
Conc., ppm	***CR*, mm y^{-1}**	**θ**	**η%**	***CR*, mm y^{-1}**	**θ**	**η%**	***CR*, mm y^{-1}**	**θ**	**η%**	***CR*, mm y^{-1}**	**θ**	**η%**
					BCPP							
100	5.81	0.71	71.22	10.32	0.70	70.12	18.34	0.67	66.92	33.91	0.63	63.42
200	4.42	0.78	78.1	8.11	0.77	76.55	14.36	0.74	74.11	27.06	0.71	70.82
300	3.04	0.85	84.95	5.54	0.84	83.95	10.06	0.82	81.85	19.51	0.79	78.95
400	1.58	0.92	92.13	3.16	0.91	90.83	6.36	0.89	88.53	13.41	0.86	85.53
500	1.02	0.95	94.95	2.61	0.92	92.42	5.37	0.90	90.32	11.66	0.87	87.42

This led to improved %η along the rise in dosages [34]. Later on after optimum concentration (500 ppm) of inhibitor, increase in concentration of the inhibitor in test solution may tend to emit small amount of already adsorbed inhibitors on N80 steel, open surface and going back into the medium leaving the N80 steel surface bare to the corrosive surrounding and leading to minor fall in %η [35]. From the Table 1, it is also evident that when test solution temperature rises, *CR* rises and protection efficiency falls. This could be because of desorption of BMPP and BCPP molecules from the NS facet. As a result, the inhibition efficiency dropped and the *CR* increased [35, 36].

The inhibitor BMPP offered higher inhibition efficacy than BCPP for all concentrations and temperatures. The structure of BMPP and BCPP are almost same and both have nearly same size and number of active centers, only the structural difference between the two inhibitors is that BMPP contains $-OCH_3$ substituent on phenyl ring whereas BCPP contains –Cl substituent on phenyl ring present in these inhibitors. Thus, the difference in corrosion inhibition efficiency between BMPP and BCPP is due to different nature of these substituent's ($-OCH_3$ and –Cl). The delocalized π-electron density at phenyl ring in case of BMPP increased due to electron donating nature of methoxy ($-OCH_3$) substituent whereas the electron density on phenyl ring in case of BCPP decreased due to electron withdrawing nature of chloro (–Cl) substituent. The higher delocalized π-electron density at phenyl ring in case of BMPP as compared to BCPP facilitate greater adsorption of BMPP on N80 steel surface than BCPP, leading to higher inhibition efficiency of BMPP than BCPP. Similar type of effect of substituent has been reported in literature by some authors [37]

3.2. Kinetic and thermodynamic parameters evaluation

By utilizing the gravimetric data and well-known Arrhenius Equation 4 given below, the activation energy was deduced to determine the mechanism of corrosion inhibition in the temperature range 303–333K.

$$\log CR = -\frac{E_a}{2.303RT} + \log A \quad (4)$$

Where CR signifies corrosion rate, E_a denotes activation energy, A implies preexponential factor, R denotes universal gas constant and T is absolute temperature. The plot of log CR *vs.* 1000/T (Figure 2) for BMPP and BCPP inhibitors was obtained using the gravimetric measurements data in the absence and presence of inhibitor to determine E_a values. E_a values were achieved by utilizing the slope of Figure 2 using the equation $E_a = -(\text{slope}\cdot 2.303\cdot R)$, obtained values are given in Table 2. It can be observed from the Table 2 that with the simultaneous rise in inhibitor concentration in the test solution, E_a values were increasing for BMPP and BCPP inhibitors. It is reported that low E_a magnitude are related with high rate of corrosion and large E_a values are linked with low rate of corrosion. Additionally, it is also mentioned that when E_a remains constant or decreases in the inhibited medium *w.r.t* the blank, it is implying chemisorption, and when E_a increased in the medium with inhibitor presence *w.r.t* blank it implies physisorption as well as mixed adsorption [38, 39]. Increasing E_a values in this case implies that simultaneous addition of the inhibitors in the test solution decreases the rate of N80 steel dissolution in the medium due to gradual adsorption of the molecules of inhibitor on N80 steel. Similarly, Equation 5 was used to determine ΔS^* (entropy of activation) and ΔH^* (enthalpy of activation variables):

$$CR = \frac{RT}{Nh}\exp\left(\frac{\Delta S^*}{R}\right)\exp\left(-\frac{\Delta H^*}{RT}\right) \quad (5)$$

where h denotes Planck's constant ($6.626\cdot 10^{-34}$ J·s), N the Avogadro's number ($6.022\cdot 10^{23}$ mol^{-1}). Here a plot of log(CR/T) *versus* 1000/T (Figure 3) was done to evaluate ΔH* and ΔS* values for the BMPP and BCPP inhibitors. Values of ΔH* were obtained by utilizing the slope of Figure 3 by using the relation $\Delta H^* = -(\text{slope}\cdot 2.303\cdot R)$. Whereas values of ΔS* were obtained by utilizing the intercept of the plot and by the relation $\Delta S^* = [(\text{intercept} - \log\{R/Nh\})\cdot 2.303\cdot \text{R}]$. The obtained values of ΔH* and ΔS* are mentioned in Table 2. The deliberate dissolution of N80 steel in the test solution was indicated by a positive value of ΔH. The higher and steadily rising positive value of ΔH* for BMPP and BCPP inhibitors in comparison to the blank indicates that the enthalpy needed for N80 steel corrosion is rising, hence corrosion reaction at the N80 steel surface slows down [40]. Increasing values of ΔS^* in the Table 2 suggest that the system was in changing state when BMPP and BCPP inhibitors were present in the test solution, suggesting that the inhibitors were organizing itself more systematically on the NS surface. Additionally, the presence of inhibitor on the N80 steel slows down the release of hydrogen ions at metallic substrate, leading to a indiscriminate configuration of the system and an increase in entropy [41, 42]. The adsorption of BMPP and BCPP inhibitors on N80 steel surface can be realized as a quasi-substitution development in which BMPP and BCPP inhibitors displaces water species adsorbed on the N80 steel [43]. ΔS^* values are

practically the sum of energies of adsorption of inhibitors particles and desorption of H_2O on the N80 steel substrate. The increase in ΔS^* values with the increase in concentration of the inhibitor in the test solution suggested that inhibitors are adsorbing on the metal substrate and ejecting the more H_2O molecules from the N80 steel surface thus high disorderness, thereby forming a protecting film and inhibiting the corrosion phenomenon [44].

The unimolecular reactions followed the thermodynamic Equation 6 [45] given as:

$$E_a - \Delta H^* = RT \quad (6)$$

as can be seen from Table 1, that E_a and ΔH^* values vary in the same way with the inhibitor concentration and the difference of E_a and ΔH^* for both studied inhibitors is very close to RT. The difference is 2.64 which is close to RT (2.48 kJ/mol) at 298 K. Therefore, N80 steel corrosion process in 15% HCl solution each without and with various concentrations of inhibitor followed a unimolecular reaction.

Table 2. The activation and thermodynamic parameters for BMPP and BCPP inhibitors on N80 steel at different temperatures.

Concentration, ppm	E_a**, kJ/mol**	ΔH^***, kJ/mol**	ΔS^***, J/mol·K**
Blank	42.35	39.71	–89.15
		BMPP	
100	50.23	47.59	–75.03
200	53.85	51.21	–67.56
300	57.05	54.40	–61.25
400	66.11	65.78	–30.42
500	68.42	66.47	–35.97
		BCPP	
100	49.21	46.56	–77.05
200	50.38	47.47	–75.40
300	51.79	49.14	–73.98
400	59.52	50.02	–51.72
500	60.66	56.88	–53.88

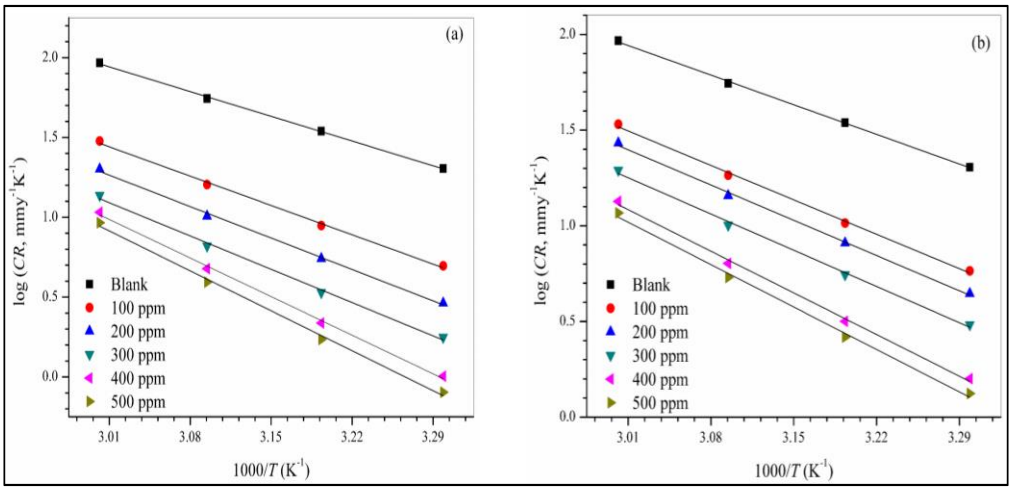

Figure 2. Plots of log *CR vs.* 1000/*T* for (a) BMPP and (b) BCPP inhibitors.

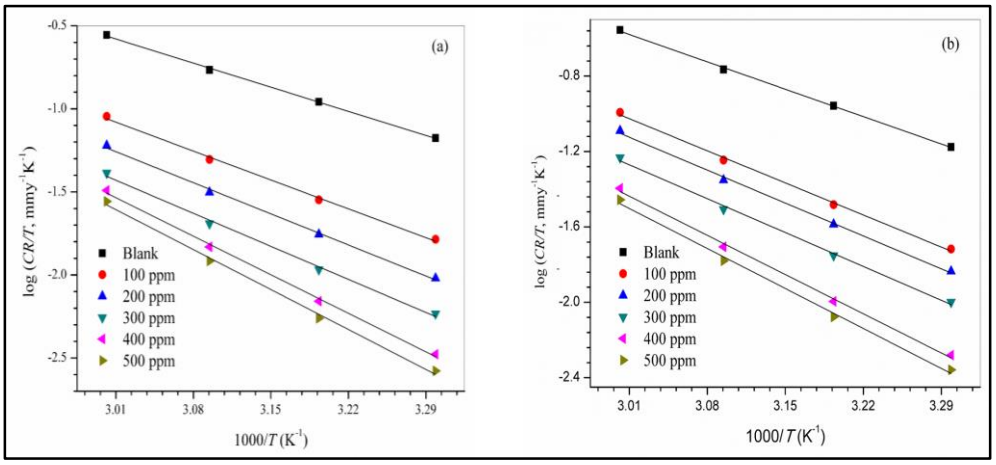

Figure 3. Plots of log *CR*/*T vs.* 1000/*T* for (a) BMPP and (b) BCPP inhibitors.

3.3. Adsorption isotherm

To determine the adsorption nature of BMPP and BCPP inhibitors on the N80 steel, different adsorption isotherm models were tested. The R^2 (correlation coefficient) values of the C_{inh}/θ *vs.* C_{inh} plot are near to perfect unity, indicating Langmuir model as the best fit isotherm model as shown in Figure 4. The virtue of Langmuir isotherm model is that molecules form a monolayer over the metal substrate and tend to have same energy, while showing no interaction with one another. C_{inh}/θ *vs.* C_{inh} plot (Langmuir) was obtained from the Equation 7.

$$\frac{C_{inh}}{\theta} = \frac{1}{K_{ads}} + C_{inh} \tag{7}$$

where C_{inh} is inhibitor concentration, K_{ads} is equilibrium constant and θ is surface coverage area. The K_{ads} (equilibrium constant) values were acquired from the intercept of plot C_{inh}/θ

vs. C_{inh} which was additionally used to ascertain ΔG_{ads} (free energy of adsorption) values exploiting the Equation 8:

$$\Delta G_{ads} = -RT \ln(55.5K_{ads}) \quad (8)$$

R = 8.314 J/mol·K, T is the temperature, and 55.5 mol/L is the concentration of H_2O.

The obtained K_{ads} and ΔG_{ads} values are listed in Table 3. The K_{ads} values reveals the level of adsorption of molecules of inhibitor on N80 steel surface which is found to be decreasing for BMPP and BCPP inhibitors, as the temperature is increased. The greater K_{ads} values of BMPP compared to BCPP inhibitors at each temperature revealed that BMPP inhibitors has better adsorption ability on N80 steel surface than BCPP inhibitors that is why BMPP inhibitors showed better inhibition efficiency than BCPP inhibitors as mentioned in gravimetric study. The negative values of ΔG_{ads} mentioned in the Table 3, illustrates the spontaneity of the process of adsorption. Since ΔG_{ads} values predict the type of adsorption whether it is physisorption or chemisorption phenomenon. The values of ΔG_{ads} for BMPP and BCPP inhibitors lies between –20 kJ/mol and –40 kJ/mol, indicating the mixed type adsorption *i.e.*, BMPP and BCPP inhibitors exhibiting both physisorption and chemisorption type of adsorption on the N80 steel surface [46, 47].

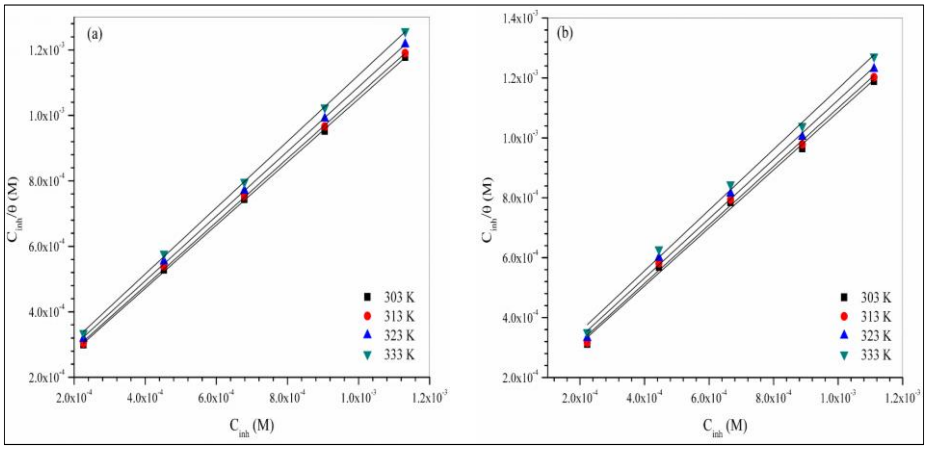

Figure 4. Plot of C_{inh}/θ *vs.* C_{inh} with or without the presence of BMPP and BCPP inhibitors for N80 steel at varied temperatures.

To further corroborate the adsorption nature for BMPP and BCPP inhibitors, parameters ΔH_{ads} (enthalpy of adsorption) and ΔS_{ads} (entropy of adsorption) were explored utilizing Equation 9:

$$\Delta G_{ads} = \Delta H_{ads} - T\Delta S_{ads} \quad (9)$$

the plot of ΔG_{ads} versus T was constructed (Figure 5). The intercept of Figure 5 provides the values of ΔH_{ads} and slope gives ΔS_{ads} as mentioned in Table 3. Since, it is mentioned in different literatures that if ΔH_{ads} values are less negative than –40 kJ/mol, adsorption phenomenon is physisorption and if it is more negative than –100 kJ/mol. adsorption phenomenon is said to be chemisorption. And if values are found between –40 kJ/mol to

–100 kJ/mol the adsorption is said to be mixed type *i.e.*, physisorption and chemisorption both [48, 49]. Here, from the values mentioned in Table 3 we can say that the mixed type of adsorption is taking place. Whereas the positive values of ΔS_{ads} reveal that increase in disordering is taking place when inhibitors BMPP and BCPP are adsorbing and forming a shielding layer on the N80 steel.

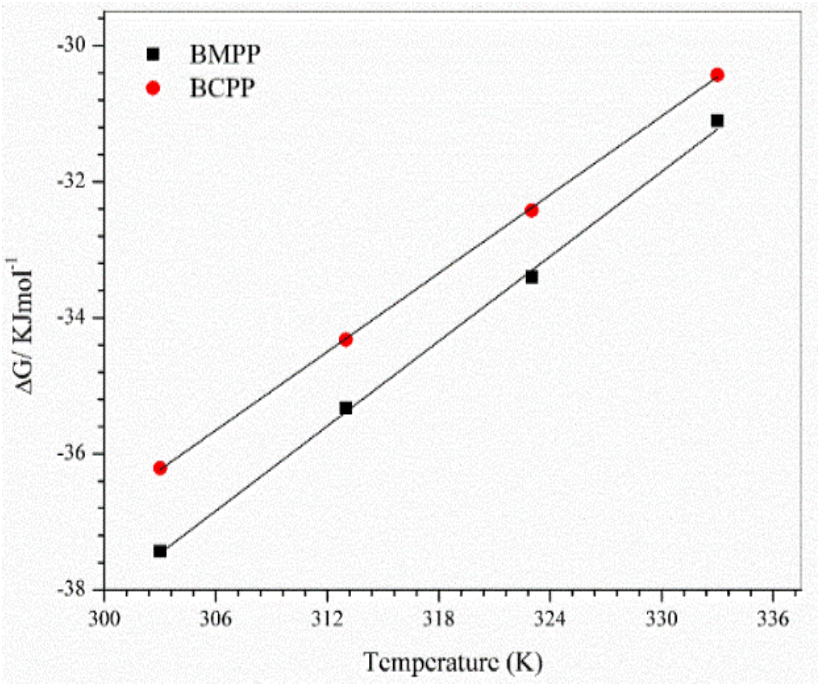

Figure 5. Plot of ΔG^0_{ads} *vs. T* for inhibitors BMPP and BCPP for N80 steel in 15% HCl.

Table 3. Adsorption factors for inhibitors BMPP and BCPP adsorption on N80 steel at varied temperatures.

Inhibitor	Temperature, K	K_{ads}, M^{-1}	ΔG_{ads}, kJ/mol	Slope	R^2	ΔH_{ads}, kJ/mol	ΔS_{ads}, J/mol
BMPP	303	51037	–37.43	1.00	0.997	–	–
	313	14168	–35.33	0.99	0.945	–	–
	323	4536	–33.40	0.95	0.993	–85	207
	333	1366	–31.11	1.04	0.992	–	–
BCPP	303	31447	–36.21	1.02	0.995	–	–
	313	9611	–34.32	0.98	0.991	–74	192
	323	3149	–32.42	1.05	0.992	–	–
	333	1068	–30.43	1.07	0.994	–	–

3.4. Electrochemical impedance measurement

The Nyquist plots for N80 steel submerged in 15% HCl solution with and without different concentrations of BMPP and BCPP are displayed in Figure 6. The Nyquist plot curves are semicircle with one peak suggesting that the corrosion of N80 steel is mostly governed by the charge transfer process. It can be seen that the diameter of the semi-circle increased as the concentration of BMPP and BCPP increased in the test solution, indicating an improvement in the corrosion protection of the N80 steel. Therefore, the capacitance semicircle can be linked to the thickness of the passive adsorbed film as well as dielectric properties. The Nyquist plot depressed semi-circle is obtained due to electrode surface heterogeneity-induced frequency dispersion [50].

The equivalent circuit shown in Figure 7 was employed to fit the experimental Nyquist plot data. CPE (constant phase element) is taken in circuit to give a best fit, in place of pure double layer capacitor (C_{dl}) [51]. Values of charge transfer resistance (R_{ct}) was obtained from the circuit and C_{dl} was obtained from CPE constant (Y_0, n) using Equation 10:

$$C_{dl} = \left(Y_0 R_{ct}^{1-n}\right)^{\frac{1}{n}} \tag{10}$$

whereas Y_0 symbolize the magnitude of CPE, R_{ct} the charge transfer resistance and n is the exponent of CPE [52].

Table 4, contains the EIS parameters, such as R_{ct} and C_{dl}, obtained from the Nyquist plots. It can be seen in Table 4, that R_{ct} values increased when concentration of BMPP and BCPP increased in the test solution due to formation of a protective layer of inhibitors between the solution and the N80 steel substrate, ultimately leads to the drop in corrosion rate of N80 steel in the test solution. As the concentration of the inhibitors BMPP and BCPP increased in the solution, decrease in the values of C_{dl} is observed, indicating that the water molecules at the electrode interface were replaced by the inhibitor molecules with lower dielectric constant. The CPE exponent n indicates surface irregularity. As seen from the Table 4, n values in presence of BMMP (0.85 to 0.97) and BCPP (0.84 to 0.95) are greater than in their absence (0.82). On increasing concentration of the inhibitors, n increased which signifies decreased surface inhomogeneity by developing an inhibitor adsorptive film on N80 steel surface [53, 54]. The %η (inhibition efficiency) values were acquired by utilizing Equation 11 and tabulated in Table 4.

$$\%\eta = \frac{R_{ct}^{i} - R_{ct}^{0}}{R_{ct}^{i}} \cdot 100 \tag{11}$$

where R_{ct}^{0} denotes charge transfer resistance of blank and R_{ct}^{i} denotes charge transfer resistance in presence of inhibitor. From the data in Table 4, it can be seen that as inhibitor concentration increased the values of %η increased. It can be observed that the %η

obtained from the EIS method and gravimetric method are compatible, demonstrating the good efficacy of the measurements.

Figure 8 shows the Bode impedance magnitude and phase angle plots for N80 steel in 15% HCl solution with and without inhibitor at open circuit potential. It can be seen in Figure 8 that single peak is observed suggesting the presence of one time constant at the N80 steel/solution interface comprising a single constant phase element. The increase in impedance magnitude with increase in inhibitor concentration suggesting the adsorption of inhibitor molecules on N80 steel surface Phase angle plots in Figure 8 showed that as the concentration of the inhibitor gradually increased, the phase angle continuously increased, suggesting gradual increase in inhibitor adsorption on the N80 steel.

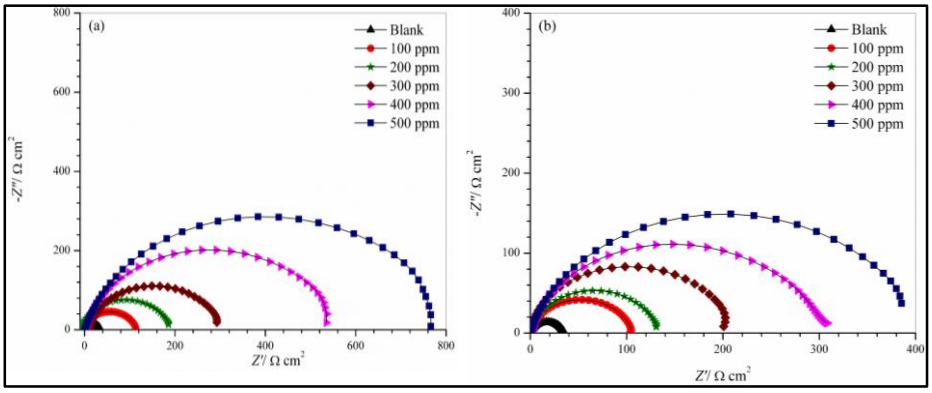

Figure 6. Nyquist plots for (a) BMPP and (b) BCPP at different concentrations for N80 steel.

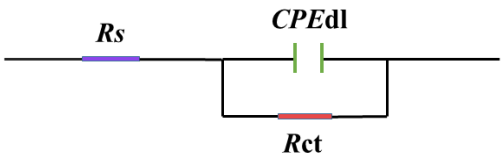

Figure 7. Equivalent circuit.

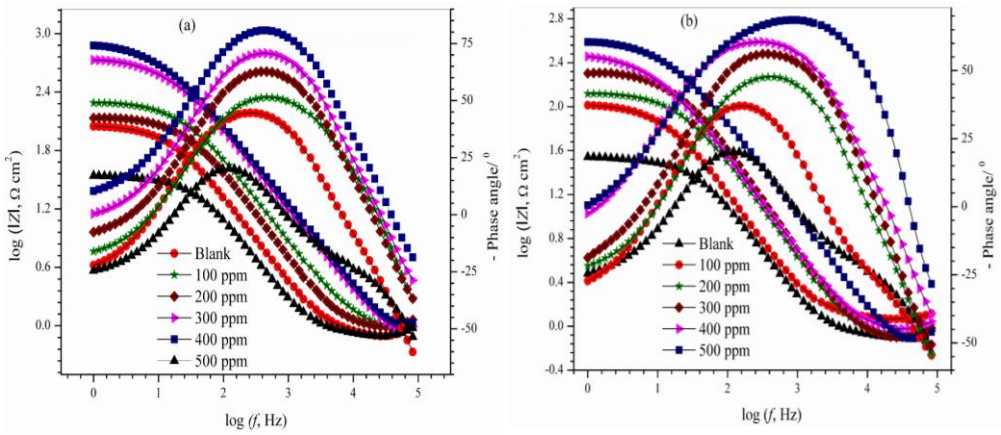

Figure 8. (a) Bode modulus and Bode phase of inhibitors (a) BMPP and (b) BCPP for N80 steel.

Table 4. Electrochemical impedance parameters of BMPP and BCPP in 15% HCl solution.

Conc., ppm	R_s, Ω·cm²	R_{ct}, Ω·cm²	Y_0, μF/cm²	n	C_{dl}, μF·cm²	%η
Blank	0.81	30	425	0.82	166.32	–
			BMPP			
100	0.84	111	246.3	0.85	118.4	73.0
200	0.86	189	164.3	0.89	95.4	84.1
300	0.89	280	132.9	0.91	90.2	89.3
400	0.73	522	87.3	0.96	75.3	94.2
500	0.93	750	67.3	0.97	60.4	96.3
			BCPP			
100	0.77	100	265.8	0.84	120.5	70.0
200	0.85	132	202.1	0.86	100.3	77.3
300	0.85	203	147.4	0.90	94.3	85.2
400	0.89	318	108.1	0.93	84.2	90.5
500	0.74	390	100.8	0.95	83.1	92.3

3.5. Potentiodynamic polarization study

The PDP curves in the absence and presence of BMPP and BCPP in the test solution, for N80 steel is shown in Figure 9. The PDP parameters obtained from the Tafel plot are tabulated in Table 5. From the Tafel plot it can be seen that the PDP curves are shifting towards lower current density after addition of either BMPP or BCPP in the testing medium, indicating that inhibitor is forming a passive layer between the N80 steel surface and acid solution which is responsible to efficiently suppress corrosion of N80 steel. The corrosion inhibition efficiency provided by the inhibitors was obtained from the Equation 12.

$$\%\eta = \frac{i_{corr}^{0} - i_{corr}^{i}}{i_{corr}^{0}} \cdot 100 \quad (12)$$

where, i_{corr}^{0} and i_{corr}^{i} denote the corrosion current density in the absence and in the presence of an inhibitor, respectively.

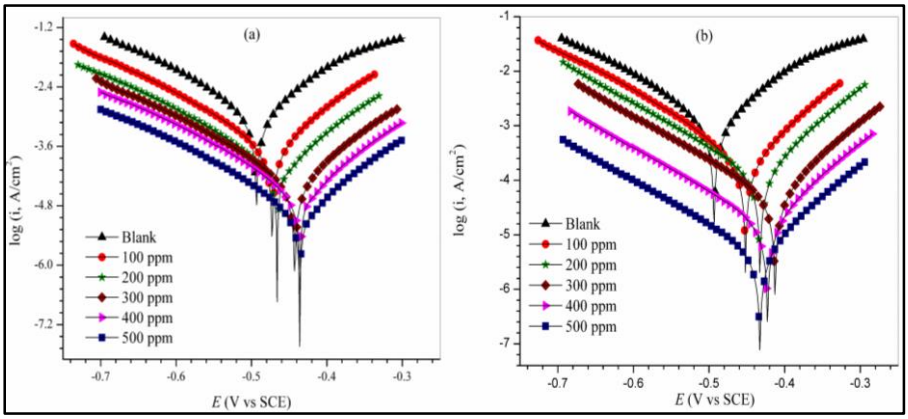

Figure 9. Tafel plots (a) BMPP and (b) BCPP in 15% HCl solution.

From Table 5 it can be observed that inhibition efficiency of both inhibitors increased on increasing the concentration due to adsorption of inhibitor molecules on N80 steel surface. The maximum %η obtained by PDP measurements for BMPP inhibitor is 96.3% at 500 ppm and in case of BCPP inhibitor it is 92.3% at 500 ppm. Figure 9, demonstrates that in presence of inhibitor an anodic shift is observed as compared to in absence of inhibitor. The observed shift in E_{corr} value in presence of inhibitor as compared to in absence of inhibitor is 80 mV. Studies have shown that if the shift in E_{corr} value in presence of inhibitor is less than ±85 mV as compared to the E_{corr} in absence of inhibitor, the inhibitor is exhibiting a mixed type inhibition regulating the anodic site's metal dissolution process and the cathodic site's hydrogen evolution reaction [55, 56]. Thus BMPP and BCPP inhibitor are mixed inhibitor with dominant anodic nature. The slight change observed in β_a and β_c values on addition of inhibitor in the test solution compared to that of blank (15% HCl) indicates that the corrosion mechanism of N80 steel remained unchanged in absence and presence of inhibitor. Both inhibitors (BMPP and BCPP) are functioning as mixed inhibitor via blocking active surface area of N80 steel by the formation of a passive film on N80 steel surface [57].

Table 5. Tafel parameters of BMPP and BCPP in 15% HCl solution.

Conc., ppm	E_{corr}, mV *vs.* SCE	β_a, mV/dec	$-\beta_c$, mV/dec	i_{corr}, μA/cm^2	%η
Blank	–492	94	112	563.4	–
		BMPP			
100	–474	88	116	146.4	74.0
200	–467	100	120	90.1	84.3
300	–443	93	125	56.3	90.1
400	–437	90	128	28.1	95.2
500	–435	95	123	20.1	96.4

Conc., ppm	E_{corr}, mV *vs*. SCE	β_a, mV/dec	$-\beta_c$, mV/dec	i_{corr}, μA/cm^2	%η
BCPP					
100	–431	89	117	169.0	70.3
200	–430	97	127	129.6	76.9
300	–412	92	116	95.8	83.2
400	–424	90	125	50.7	91.3
500	–434	94	129	37.6	93.3

3.6. FESEM study

Figure 10 provides FESEM images of uninhibited and inhibited samples. Figure 10a, depicts the image of the polished NS surface. Here fine scratches due to polishing can be seen. Figure 10b, depicts NS facet picture in presence of 15% HCl solution without inhibitor where deep scratches and corrosion pits are observed due to severe corrosion. Whereas Figure 10c and 10d, shows minor pits and scratches due adsorption of BMPP and BCPP on NS facet causing corrosion prevention. According to visualization of Figure 10c and 10d, it is clear that BMPP (Figure 10d) is a better inhibitor than BCPP (Figure 10c) due to its smoother surface.

3.7. AFM study

Figure 11 depicts the AFM images of uninhibited and inhibited specimens. Figure 11a depicts the AFM picture of polished NS facet, Figure 11b without inhibitor, Figure 11c with 500 ppm BMPP and Figure 11d 500 ppm of BCPP. The roughness value of the polished NS specimen (1.43 nm) is very low with respect to NS facet treated with 15% HCl solution without inhibitor (128 nm). This observation informing that 15% HCl solution strongly corrodes the NS facet. However, in presence BMPP and BCPP surface roughness significantly reduced to 5.37 and 14.6 nm, respectively. The lower roughness value of BMPP with respect to BCPP referred better efficacy of BMPP than BCPP.

3.8. XPS analysis

To get information regarding the elemental composition of corrosion preventing layer of BMPP and BCPP on NS facet, XPS of the specimen was done as flashed in Figure 12. The presence of peaks corresponding to the elements present in BMPP and BCPP in their corresponding XPS spectra, confirming the adsorption of BMPP and BCPP on NS facet [58].

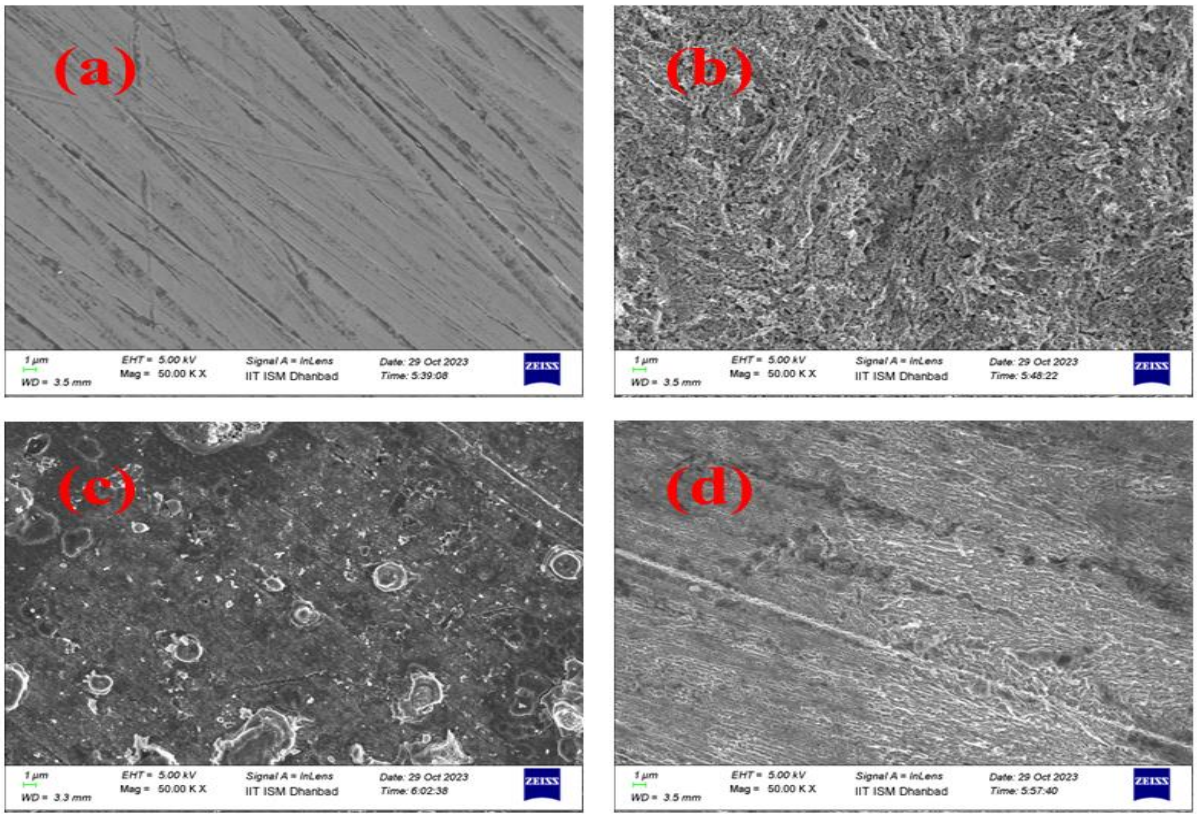

Figure 10. FESEM images of uninhibited and inhibited samples.

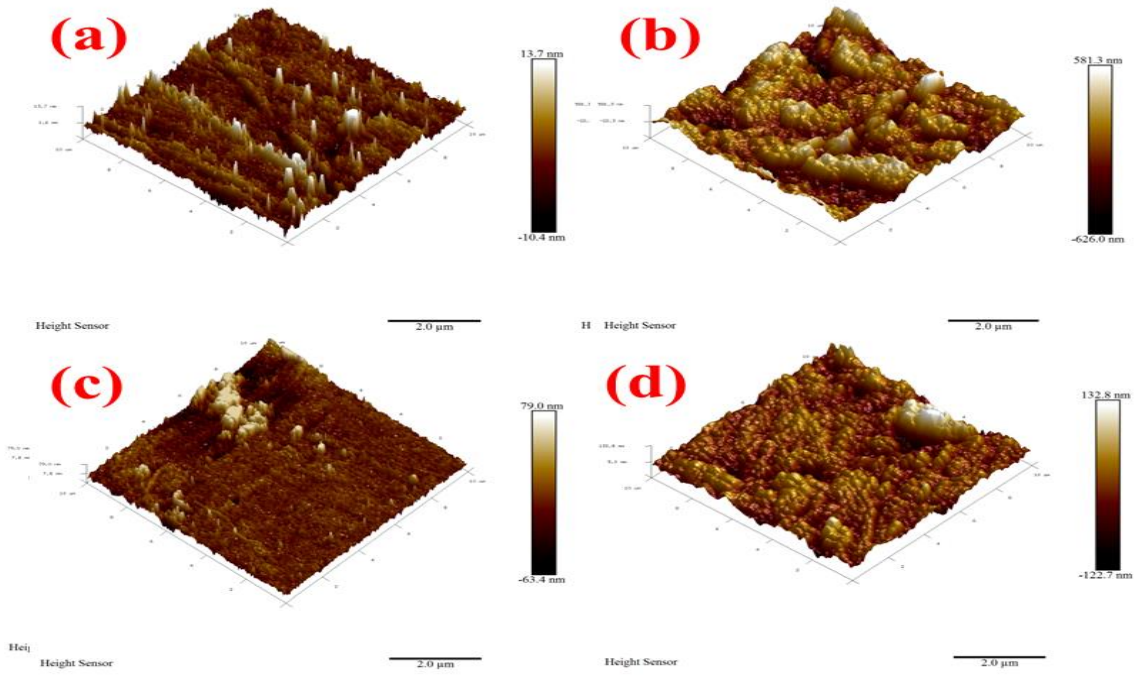

Figure 11. AFM images of uninhibited and inhibited samples.

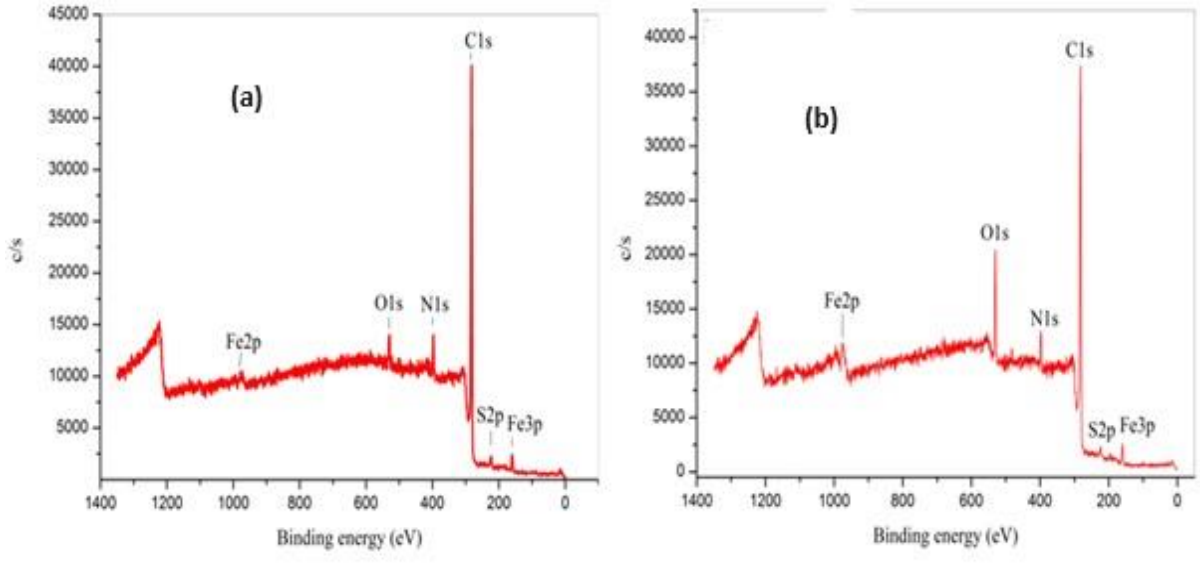

Figure 12. XPS spectra of (a) BCPP +NS (b) BMPP + NS.

3.9. DFT calculations

DFT was performed on both inhibitors is gas as well as in aqueous phase and different parameters were calculated. HOMO and LUMO of BMPP and BCPP optimized structures in gas and aqueous phases are flashed in Figures 13 and 14, and Table 6 illustrates the related quantum chemical parameters.

Using E_{HOMO} and E_{LUMO} the value of ΔE (energy gap), S (chemical softness), η (chemical hardness), χ (absolute electronegativity), and ΔN (electron transfer from the inhibitor to NS facet), were obtained using the mathematical Equations 13 to 16 [59] and obtained values are listed in Table 6.

$$\Delta E = E_{LUMO} - E_{HOMO} \tag{13}$$

$$\chi = \frac{-(E_{LUMO} + E_{HOMO})}{2} \tag{14}$$

$$\eta = \frac{E_{LUMO} - E_{HOMO}}{2} \tag{15}$$

$$S = \frac{1}{\eta} \tag{16}$$

According to Kokalj [60], fraction of transferred electrons (ΔN) from the inhibitor to the mild steel surface or mild steel surface to inhibitor can be calculated with the help of work function (ϕ) and η values, using the Equation given below:

$$\Delta N = \frac{\phi - \chi_{inh}}{2\eta_{inh}} \tag{17}$$

where ϕ for Fe is taken as 4.82 eV/mol [61, 62].

As stated by the FMO hypothesis, HOMO and LUMO energies provide information regarding the electron donating and accepting character of corrosion inhibitor [44]. According to literature reports, corrosion protecting compounds with high E_{HOMO} and low E_{LUMO} favours incredibly high effectiveness. Similar to this, the low energy gap (ΔE) is a crucial factor of corrosion preventing compound to suppress corrosion because it accelerates adsorption [63]. As shown in Table 6, BMPP has a low ΔE value, with respect to BCPP in aqueous as well as in gas phase, which supports the higher efficiency of BMPP for being adsorbed on NS and showing higher efficacy with respect to BCPP [37]. Furthermore, the low electronegativity values (χ) favors increased efficacy of the corrosion preventing compound because of low electrons giving character to the NS facet [37]. Additionally, the softness (S) and hardness (η) of the corrosion preventing compound are also crucial factors, low η and high S favor high corrosion preventive ability of the compound. As it is known that Fe is soft, therefore compound with high S and low η will strongly adsorb at NS facet, as per HSAB principle. According to Table 6, BMPP exhibits lower η and higher S values in both gas as well as in aqueous phase with respect to BCPP which clearly denotes a greater corrosion preventive ability of BMPP with respect to BCPP. The larger the ΔN value further suggests the good protection of NS facet [63]. The probability of the tested compounds BMPP and BCPP to donate or accept electrons to the NS facet is measured by the ΔN values. A back-donation of electrons from the NS facet to inhibitor suggests negative ΔN whereas positive value informs the electron donation from corrosion preventing compound to NS facet [64]. According to Table 6, both BMPP and BCPP show positive value and BMPP shows higher value with respect to BCPP, therefore corrosion preventive ability of BMPP is higher with respect to BCPP. [64]. The dipole moment (μ) of corrosion preventive compound is another important parameter that helps in deciding corrosion prevention [63]. The rise in μ improves adsorption of corrosion preventing compound on NS facet because of higher electrostatic force of attraction between the corrosion preventing compound and NS facet. As a result, an increase in dipole moment values enhanced the corrosion prevention [59].

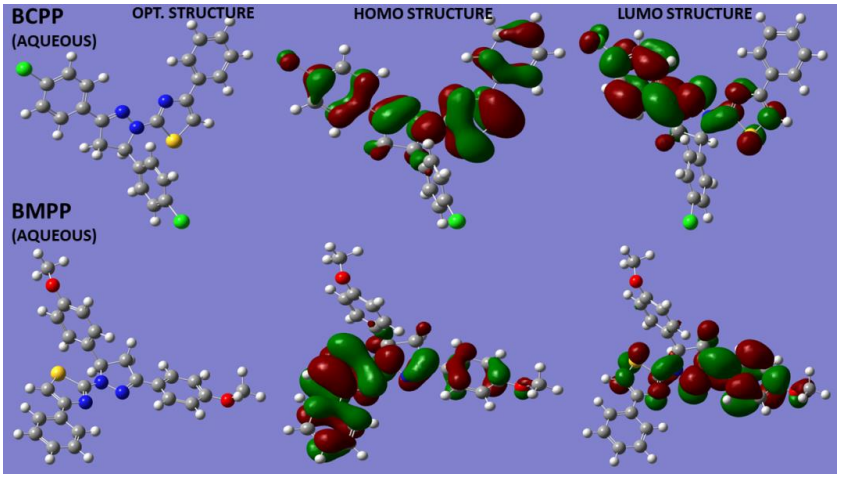

Figure 13. BMPP and BCPP in aqueous phase.

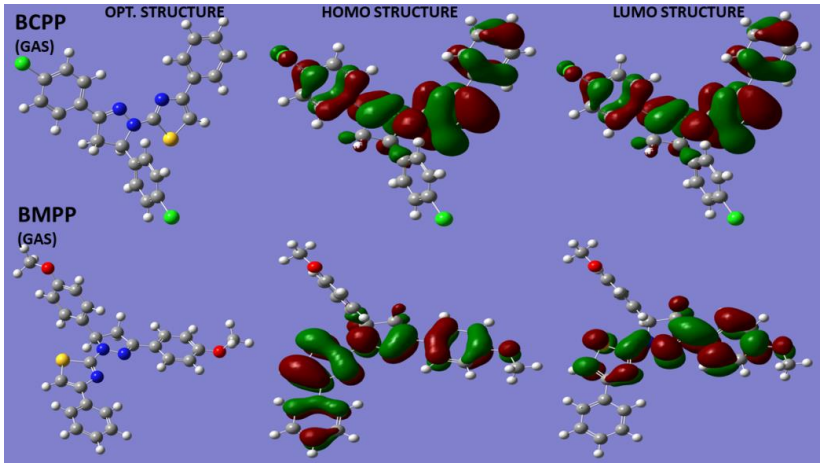

Figure 14. BMMP and BCPP in gas phase.

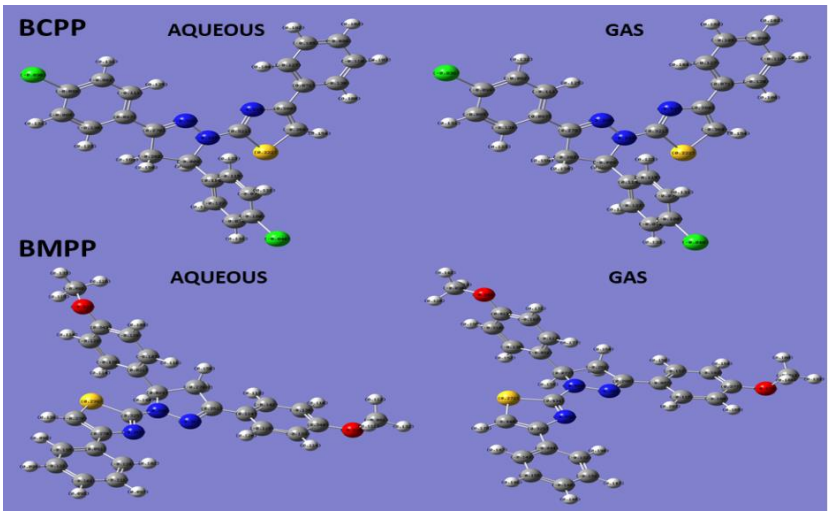

Figure 15. Mulliken charges of BMPP and BCPP in aqueous phase.

Table 6. Quantum chemical descriptors for molecules PBTP and FPBP.

System	E_{HOMO}, eV	E_{LUMO}, eV	ΔE, eV	η	S	χ	μ, D	ΔN
BMPP(Aqu)	–5.224	–2.126	3.098	1.549	0.646	3.675	6.85	0.3696
BMPP (Gas)	–4.841	1.428	3.413	1.707	0.586	3.135	5.25	0.4937
BCPP (Aqu)	–5.320	1.628	3.692	1.846	0.542	3.474	6.46	0.3646
BCPP (Gas)	–5.243	–1.605	3.638	1.819	0.549	3.424	5.12	0.3837

The Mulliken charges on different elements present in BMPP and BCPP in gas and aqueous phase are portrayed in Figure 15. It can be visualized from Figure 15 that some elements exhibited positive charge and others have negative charge. A careful observation of Figure 15 reflects that atoms N, O, Cl and some C bear negative charges, which gives the information that these elements are the active sites of BMPP and BCPP for adsorption on NS facet [59].

4. Corrosion Inhibition Mechanism

The results obtained from studies executed to assess the corrosion preventive ability of BMPP and BCPP, suggested that both compounds prevent corrosion of NS facet effectively in 15% HCl solution. When BMPP and BCPP comes in contact to NS in 15% HCl solution, strongly adsorbed on its surface and prevent its corrosion. The reason of strong adsorption is the presence of N, S, O and pi-electrons in both compounds. When these compounds are added in 15% HCl solution, they become positively charged (protonated) and generate strong attractive force with Cl^- already present on NS surface and facilitate their adsorption through physisorption on NS facet [65]. When these compounds are in non-protonated state they adsorb on NS facet by giving their lone paired electrons situated at heteroatoms to unfilled d-orbital of Fe on NS facet resulting in chemisorption [59]. Thus, adsorption of BMPP and BCPP on NS surface occurs through physisorption as well as chemisorption. The adsorption of inhibitor molecules on NS surface is responsible for corrosion prevention of NS in 15% HCl solution.

5. Conclusions

Overall, it is concluded that BMPP and BCPP exhibit good corrosion preventive ability towards NS in 15% HCl solution and offered 97.98 and 94.95 percent corrosion preventive efficacy at 500 ppm. Both BMPP and BCPP exhibited mixed adsorption over NS facet and their adsorption obeyed Langmuir isotherm. According to PDP, presence of BMPP and BCPP in 15% HCl solution influenced anodic and cathodic reactions and showed mixed nature. The FESEM, AFM and XPS measurements validate the formation of protective inhibitor film responsible for NS corrosion prevention in acidic solution. DFT findings validate the experimental results.

Declaration of Competing Interest

Authors have no competing interests to declare.

References

1. M. Finsgar and J. Jackson, Application of corrosion inhibitors for steels in acidic media for the oil and gas industry: A review, *Corros. Sci*., 2014, **86**, 17–41. doi: 10.1016/j.corsci.2014.04.044
2. N.M. El Basiony, E.E. Badr, S.A. Baker and A.S. El-Tabei, Experimental and theoretical (DFT & MC) studies for the adsorption of the synthesized Gemini cationic surfactant based on hydrazide moiety as X-65 steel acid corrosion inhibitor, *Appl. Surf. Sci*., 2021, **539**, 148246. doi: 10.1016/j.apsusc.2020.148246
3. A.S.H. Makhlouf, V. Herrera and E. Munoz, Corrosion and protection of the metallic structures in the petroleum industry due to corrosion and the techniques for protection, *Handb. Mater. Failure Anal. Case Stud. Chem., Concr. Power Ind*., 2018, 107–122. doi: 10.1016/B978-0-08-101928-3.00006-9

4. M.A. Quraishi, N. Sardar and H. Ali, A Study of Some New Acidizing Inhibitors on Corrosion of N-80 Alloy in 15% Boiling Hydrochloric Acid, *Corrosion*, 2002, **58**, no. 4, 317–321. doi: 10.5006/1.3287679
5. Emranuzzaman, T. Kumar, S. Vishawanatam and G. Udaybhanu, Synergistic effects of formaldehyde and alcoholic extract of plant leaves for protection of N80 steel in 15% HCl, *Corros. Eng. Sci. Technol*., 2004, **39**, 327–332. doi: 10.1179/174327804X13181
6. M. Yadav, D. Behera and U. Sharma, Nontoxic corrosion inhibitors for N80 steel in hydrochloric acid, *Arabian J. Chem*., 2016, **9**, S1487–S1495. doi: 10.1016/j.arabjc.2012.03.011
7. S. Kumar, D. Sharma, P.N. Yadav and M. Yadav, Experimental and Quantum Chemical Studies on Corrosion Inhibition Effect of Synthesized Organic Compounds on N80 Steel in Hydrochloric Acid, *Ind. Eng. Chem. Res*., 2013, **52**, 14019–14029. 10.1021/acs.iecr.8b02960
8. Y. Yang, N. Ali, M. Bilal, A. Khan, F. Ali, P. Mao, L. Ni, X. Gao, K. Hong, K. Rasool and H.M.N. Iqbal, Robust membranes with tunable functionalities for sustainable oil/ water separation, *J. Mol. Liq*., 2021, **321**, 114701. doi: 10.1016/j.molliq.2020.114701
9. B. Chugh, S. Thakur, B. Pani, M. Murmu, P. Banerjee, A.M. Al-Mohaimeed, E.E. Ebenso, M. Singh, J. Singh and A.K. Singh, Investigation of phenol-formaldehyde resins as corrosion impeding agent in acid solution, *J. Mol. Liq*., 2021, **330**, 115649. doi: 10.1016/j.molliq.2021.115649
10. A. Elyoussfi, H. Outada, J. Issad, H. Lrhoul, A. Salhi and A. Dafali, Corrosion inhibitors of alloysand metals in acidic solution: Abibliometric analysis from 2010 to 2022, *Int.J. Corros. Scale Inhib*., 2023, **12**, no. 2, 722–740. doi: 10.17675/2305-6894-2023-12-2-19
11. M.D. Plotnikova, A.B. Shein, M.G. Scherban, A.N. Vasyanin and A.E. Rubtsov, Experimental and theoretical investigation of (E)-5-{[4-(dimethylamino)benzylidene] amino}-1,3,4-thiadiazole-2(3H)-thione (DATT) as an acid corrosion inhibitor of mild steel, *Int. J. Corros. Scale Inhib*., 2023, **12**, no. 4, 1365–1391. doi: 10.17675/2305-6894-2023-12-4-1
12. N. Dheer, A.K. Kalra, D. Singh, S.K. Ujjain, P. Ahuja, R. Kumar, P. Singh, N.K. Johar, M.R. Singh and R. Kanojia, Mild steel corrosion inhibition by nicotinamide as a green inhibitor: An electrochemical, thermodynamic and theoretical insight, *Int. J. Corros. Scale Inhib*., 2023, **12**, no. 4, 1645–1667. doi: 10.17675/2305-6894-2023-12-4-13
13. G. Ji, S. Anjum, S. Sundaram and R. Prakash, Paradisica peel extract as green corrosion inhibitor for mild steel in HCl solution, *Corros. Sci*., 2015, **90**, 107–117. doi: 10.1016/j.corsci.2014.10.002
14. C. Verma, V.S. Saji, M.A. Quraishi and E.E. Ebenso, Pyrazole derivatives as environmental benign acid corrosion inhibitors for mild steel: Experimental and computational studies, *J. Mol. Liq*., 2020, **298**, 111943. doi: 10.1016/j.molliq.2019.111943

15. C. Verma, L.O. Olasunkanmi, E.E. Ebenso, M.A. Quraishi and I.B. Obot, Adsorption behavior of glucosamine-based, pyrimidine-fused heterocycles as green corrosion inhibitors for mild steel: experimental and theoretical studies, *J. Phys. Chem. C*, 2016, **120**, no. 21, 11598–11611. doi: 10.1021/acs.jpcc.6b04429
16. A. Alamiery, E. Mahmoudi and T. Allami, Corrosion inhibition of low-carbon steel in hydrochloric acid environment using a Schiff base derived from pyrrole: gravimetric and computational studies, *Int. J. Corros. Scale Inhib*., 2021, **10**, no. 2, 749–765. doi: 10.17675/2305-6894-2021-10-2-17
17. Y.M. Abdulsahib, A.J.M. Eltmimi, S.A. Alhabeeb, M.M. Hanoon, A.A. AlAmiery, T. Allami and A.A.H. Kadhum, Experimental and theoretical investigations on the inhibition efficiency of N-(2,4-dihydroxytolueneylidene)-4-methylpyridin-2-amine for the corrosion of mild steel in hydrochloric acid, *Int. J. Corros. Scale Inhib*., 2021, **10**, no. 3, 885–899. doi: 10.17675/2305-6894-2021-10-3-3
18. J.V. Faria, P.F. Vegi, A.G.C. Miguita, M.S. dos Santos, N. Boechat and A.M.R. Bernardino, Recently reported biological activities of pyrazole compounds, *Bioorg. Med. Chem*., 2017, **25**, no. 21, 5891–5903. doi: 10.1016/j.bmc.2017.09.035
19. A.D. Kumar, S. Bharath, R.N. Dharmappa, S. Naveen, N.K. Lokanath and K.A. Kumar, Synthesis and spectroscopic and crystallographic characterisation of novel functionalized pyrazole derivatives: biological evaluation for their cytotoxic, angiogenic and antioxidant activities, *Res. Chem. Intermed*., 2018, **44**, 5635–5652. doi: 10.1007/s11164-018-3445-6
20. A.D. Kumar, M.G. Prabhudeva, S. Bharath, K. Karthik, N.K. Lokanath and K.A. Kumar, Design and Amberlyst-15 mediated synthesis of novel thienylpyrazole carboxamides that potently inhibit Phospholipase A2 by binding to an allosteric site on the enzyme, *Bioorg. Chem*., 2018, **80**, 444–452. doi: 10.1016/j.bioorg.2018.06.023
21. A. Sehmi, H.B. Ouici, A. Guendouzi, M. Ferhat, O. Benali and F. Boudjellal, Corrosion Inhibition of Mild Steel by newly Synthesized Pyrazole Carboxamide Derivatives in HCl Acid Medium: Experimental and Theoretical Studies, *J. Electrochem. Soc*., 2020, **167**, 155508. doi: 10.1149/1945-7111/abab25
22. G. Laadam, F. Benhiba, M. El Faydy, A. Titi, A.S. Al-Gorair, M. Alshareef, H. Hawsawi, R. Touzani, I. Warad, A. Bellaouchou, A. Guendouzi, M. Abdallah and A. Zarrouk, Anti-corrosion performance of novel pyrazole derivative for carbon steel corrosion in 1 M HCl: Computational and experimental studies, *Inorg. Chem. Commun*, 2022, **145**, 109963. doi: 10.1016/j.inoche.2022.109963
23. G. Laadam, M. El Faydy, F. Benhiba, A. Titi, H. Amegroud, A.S. Al-Gorair, H. Hawsawi, R. Touzani, I. Warad, A. Bellaouchou, A. Guendouzi, M. Abdallah and A. Zarrouk, Outstanding anti-corrosion performance of two pyrazole derivatives on carbon steel in acidic medium: Experimental and quantum-chemical examinations, *J. Mol. Liq*., 2023, **375**, 121268. doi: 10.1016/j.molliq.2023.121268
24. M.M. Shaban, N.M. El Basiony, A.B. Radwan, E.E. El-Katori, A. Abu-Rayyan, N.H. Bahtiti and M.M. Abdou, Electrochemical Investigation of C-Steel Corrosion

Inhibition, In Silico, and Sulfate-Reducing Bacteria Investigations Using Pyrazole Derivatives, *ACS Omega*, 2023, **8**, no. 33, 30068–30080. doi: 10.1021/acsomega.3c02333
25. K. Cherraka, M.E. Belghitia, A. Berrissoula, M. El Massaoudia, M. El Faydyb, M. Talebc, S. Radia, A. Zarroukd and A. Dafalia, Pyrazole carbohydrazide as corrosion inhibitor for mild steel in HCl medium: Experimental and theoretical investigations, *Surf. Interfaces*, 2020, **20**, 10057. doi: 10.1016/j.surfin.2020.100578
26. M. Yadav, R.R. Sinha, T.K. Sarkar and N. Tiwari, Corrosion inhibition effect of pyrazole derivatives on mild steel in hydrochloric acid solution, *J. Adhes. Sci. Technol*., 2015, **29**, 1690–1713. doi: 10.1080/01694243.2015.1040979
27. G.T. Zitouni, P. Chevallet, F.S. Kiliç and K. Erol, Synthesis of some thiazolyl-pyrazoline derivatives and preliminary investigation of their hypotensive activity, *Eur. J. Med. Chem*., 2000, **35**, no. 6, 635–641. doi: 10.1016/S0223-5234(00)00152-5
28. A.A. Bilgin, E. Palaska and R. Sunal, Studies on the synthesis and antidepressant activity ofsome-1-thiocarbamoyl-3,5-diphenyl-2-pyrazolines, *Arzneimittel-forschung*, 1993, **43**, 1041–1044.
29. ASTM G. 31–72. Standard Practice for Laboratory Immersion Corrosion Testing of Metals; ASTM, 1990.
30. P.K. Paul, M. Yadav and I.B. Obot, Investigation on corrosion protection behavior and adsorption of carbohydrazide-pyrazole compounds on mild steel in 15% HCl solution: electrochemical and computational approach, *J. Mol. Liq*., 2020, **314**, 113513. doi: 10.1016/j.molliq.2020.113513
31. M.J. Frisch, G.W. Trucks, H.B. Schlegel, G.E. Scuseria, M.A. Robb, J.R. Cheeseman, G. Scalmani, V. Barone, B. Mennucci, G.A. Petersson, H. Nakatsuji, M. Caricato, X. Li, H.P. Hratchian, A.F. Izmaylov, J. Bloino, G. Zheng, J.L. Sonnenberg, M. Hada, M. Ehara, K. Toyota, R. Fukuda, J. Hasegawa, M. Ishida, T. Nakajima, Y. Honda, O. Kitao, H. Nakai, T. Vreven, J.A. Montgomery, Jr. J.E. Peralta, F. Ogliaro, M. Bearpark, J.J. Heyd, E. Brothers, K.N. Kudin, V.N. Staroverov, R. Kobayashi, J. Normand, K. Raghavachari, A. Rendell, J.C. Burant, S.S. Iyengar, J. Tomasi, M. Cossi, N. Rega, J.M. Millam, M. Klene, J.E. Knox, J.B. Cross, V. Bakken, C. Adamo, J. Jaramillo, R. Gomperts, R.E. Stratmann, O. Yazyev, A.J. Austin, R. Cammi, C. Pomelli, J.W. Ochterski, R.L. Martin, K. Morokuma, V.G. Zakrzewski, G.A. Voth, P. Salvador, J.J. Dannenberg, S. Dapprich, A.D. Daniels, Ö. Farkas, J.B. Foresman, J.V. Ortiz, J. Cioslowski and D.J. Fox, *Gaussian 09, Revision C.01*, Gaussian, Inc., Wallingford CT, 2009.
32. J. Tirado-Rives and W.L. Jorgensen, Performance of B3LYP Density Functional Methods for a large set of organic molecules, *J. Chem. Theory Comput*., 2008, **4**, no. 2, 297–306. doi: 10.1021/ct700248k
33. J.R. Dennington, T.K. Millam, R. Dennington, T. Keith and J. Millam, *GaussView; 131 TS*, Semichem Inc., Shawnee, KS, USA, 2009.
34. M. Mobin, I. Ahmad, M. Basik, M. Murmu and P. Banerjee, Experimental and theoretical assessment of almond gum as an economically and environmentally viable

corrosion inhibitor for mild steel in 1 M HCl, *Sustainable Chem. Pharm.*, 2020, **18**, 100337. doi: 10.1016/j.scp.2020.100337
35. D.K. Yadav and M.A. Quraishi, Application of Some Condensed Uracils as Corrosion Inhibitors for Mild Steel: Gravimetric, Electrochemical, Surface Morphological, UV–Visible, and Theoretical Investigations, *Ind. Eng. Chem. Res.*, 2012, **51**, no. 46, 14966–14979. doi: 10.1021/ie301840y
36. M. Mobin, I. Ahmad and M. Shoeb, Investigation into the highly efficient Artemisia absinthium-silver nanoparticles composite as a novel environmentally benign corrosion inhibitor for mild steel in 1 M HCl, *J. Adhes. Sci and Technol.*, 2022, **36**, 2562–2587. doi: 10.1080/01694243.2022.2075523
37. M. Yadav, R.R. Sinha, S. Kumar and T.K. Sarkar, Corrosion inhibition effect of spiropyrimidinethiones on mild steel in 15% HCl solution: insight from electrochemical and quantum studies, *RSC Adv.*, 2015, **5**, 70832–70848. doi: 10.1039/C5RA14406J
38. R.K. Mehta, S.K. Gupta and M. Yadav, Studies on pyrimidine derivative as green corrosion inhibitor in acidic environment: Electrochemical and computational approach, *J. Environ. Chem. Eng.*, 2022, **10**, 108499. doi: 10.1016/j.jece.2022.108499
39. M. Mobin, I. Ahmad, M. Murmu, Priyabrata Banerjee, and Ruby Aslam, Corrosion inhibiting properties of polysaccharide extracted from Lepidium meyenii root for mild steel in acidic medium: Experimental, density functional theory, and Monte Carlo simulation studies, *J. Phys. Chem. Solids*, 2023, **179**, 111411. doi: 10.1016/j.jpcs.2023.111411
40. R. Kumar, O.S. Yadav and G. Singh, Electrochemical and surface characterization of a new eco-friendly corrosion inhibitor for mild steel in acidic media: A cumulative study, *J. Mol. Liq.*, 2017, **237**, 413–427. doi: 10.1016/j.molliq.2017.04.103
41. Z. Tao, W. He, S. Wang, S. Zhang and G. Zhou, A study of differential polarization curves and thermodynamic properties for mild steel in acidic solution with nitrophenyltriazole derivative, *Corros. Sci.*, 2012, **60**, 205–213. doi: 10.1016/j.corsci.2012.03.035
42. M. Mobin, M. Basik and J. Aslam, Boswellia serrata gum as highly efficient and sustainable corrosion inhibitor for low carbon steel in 1 M HCl solution: Experimental and DFT studies, *J. Mol. Liq.*, 2018, **263**, 174–186. doi: 10.1016/j.molliq.2018.04.150
43. A.K. Singh and M.A. Quraishi, Effect of Cefazolin on the corrosion of mild steel in HCl solution, *Corros. Sci.*, 2010, **52**, 152–160. doi: 10.1016/j.corsci.2009.08.050
44. S.M.A. Hosseini and A. Azimi, The inhibition of mild steel corrosion in acidic medium by 1-methyl-3-pyridin-2-yl-thiourea, *Corros. Sci.*, 2009, **51**, 728–732. doi: 10.1016/j.corsci.2008.11.019
45. A. Alamiery, Corrosion inhibition effect of 2-N-phenylamino-5-(3-phenyl-3-oxo-1-propyl)-1,3,4-oxadiazole on mild steel in 1 M hydrochloric acid medium: Insight from gravimetric and DFT, *Mater. Sci. Energy Technol.*, 2021, **4**, 398–406. doi: 10.1016/j.mset.2021.09.002

46. M.H. Sliem, N.M. El Basiony, E.G. Zaki, M.A. Sharaf and A.M. Abdullah, Corrosion inhibition of mild steel in sulfuric acid by a newly synthesized Schiff base: an electrochemical, DFT, and Monte Carlo simulation study, *Electroanalysis*, 2020, **32**, 3145–3158. doi: 10.1002/elan.202060461
47. Y. Sasikumar, A.S. Adekunle, L.O. Olasunkanmi, I. Bahadur, R. Baskar, M.M. Kabanda, I.B. Obot and E.E. Ebenso, Experimental, quantum chemical and Monte Carlo simulation studies on the corrosion inhibition of some alkyl imidazolium ionic liquids containing tetrafluoroborate anion on mild steel in acidic medium, *J. Mol. Liq.*, 2015, **211**, 105–118. doi: 10.1016/j.molliq.2015.06.052
48. F. Bentiss, M. Lebrini and M. Lagrenee, Thermodynamic characterization of metal dissolution and inhibitor adsorption processes in mild steel/2,5-bis(n-thienyl)- 1,3,4 thiadiazoles/hydrochloric acid system, *Corros. Sci.*, 2005, **47**, 2915–2931. doi: 10.1016/j.corsci.2005.05.034
49. T.K. Sarkar, V. Saraswat, R.K. Mitra, I.B. Obot and M. Yadav, Mitigation of corrosion in petroleum oil well/tubing steel using pyrimidines as efficient corrosion inhibitor: Experimental and theoretical investigation, *Mater. Today Commun.*, 2021, **26**, 101862. doi: 10.1016/j.mtcomm.2020.101862
50. B.D. Mert, A.O. Yüce, G. Kardas and B. Yazıcı, Inhibition effect of 2-amino-4-methylpyridine on mild steel corrosion: experimental and theoretical investigation, *Corros. Sci.*, 2014, **85**, 287–295. doi: 10.1016/j.corsci.2014.04.032
51. M. Mobin, I. Ahmad, R. Aslam and M. Basik, Characterization and application of almond gum-silver nanocomposite as an environmentally benign corrosion inhibitor for mild steel in 1 M HCl, *Mater. Chem. Phys*, 2022, **289**, 126491. doi: 10.1016/j.matchemphys.2022.126491
52. J. Cui, Y. Yang, X. Li, W. Yuan and Y. Pei, Toward a slow-release borate inhibitor to control mild steel corrosion in simulated recirculating water, *ACS Appl. Mater. Interfaces*, 2018, **10**, 4183–4197. doi: 10.1021/acsami.7b15507
53. Y. Qiang, S. Zhang, B. Tan and S. Chen, Evaluation of Ginkgo leaf extract as an eco-friendly corrosion inhibitor of X70 steel in HCl solution, *Corros. Sci.*, 2018, **133**, 6–16. doi: 10.1016/j.corsci.2018.01.008
54. M. Ramezanzadeh, G. Bahlakeh, Z. Sanaei and B. Ramezanzadeh, Corrosion inhibition of mild steel in 1 M HCl solution by ethanolic extract of eco-friendly Mangifera indica (mango) leaves: Electrochemical, molecular dynamics, Monte Carlo and ab initio study, *Appl. Surf. Sci.*, 2019, **463**, 1058–1077. doi: 10.1016/j.apsusc.2018.09.029
55. O.S.I. Fayomi, I.G. Akande, A.P.I. Popoola, S.I. Popoola and D. Daramola, Structural characterization and corrosion properties of electroless processed Ni–P–MnO_2 composite coatings on SAE 1015 steel for advanced applications, *J. Sci. Adv. Mater. Devices*, 2019, **4**, 285–289. doi: 10.1016/j.jsamd.2019.04.001
56. E. Kowsari, S.Y. Arman, M.H. Shahini, H. Zandi, A. Ehsani, R. Naderi, A. PourghasemiHanza and M. Mehdipour, In situ synthesis, electrochemical and quantum chemical analysis of an amino acid-derived ionic liquid inhibitor for corrosion

protection of mild steel in 1M HCl solution, *Corros. Sci*., 2016, **112**, 73–85. doi: 10.1016/j.corsci.2016.07.015
57. D.B. Tripathy, M. Murmu, P. Banerjee and M.A. Quraishi, Palmitic acid based environmentally benign corrosion inhibiting formulation useful during acid cleansing process in MSF desalination plants, *Desalination*, 2019, **472**, 114128. doi: 10.1016/j.desal.2019.114128
58. M. Yadav, R.R. Sinha, S. Kumar and T.K. Sarkar, Corrosion inhibition effect of spiropyrimidinethiones on mild steel in 15% HCl solution: insight from electrochemical and quantum studies, *RSC Adv*., 2015, **5**, 70832–70848. doi: 10.1039/C5RA14406J
59. S.K. Gupta, R.K. Mehta, N. Kumari, M. Yadav and I.B. Obot, Study on benzylidine derivatives as corrosion inhibitors for mild steel in 15% HCl medium: Experimental and theoretical investigation, *J. Phys. Chem. Solids*, 2023, **183**, 111632. doi: 10.1016/j.jpcs.2023.111632
60. A. Kokalj, On the HSAB based estimate of charge transfer between adsorbates and metal surfaces, *Chem. Phys*., 2012, **393**, 1–12. doi: 10.1016/j.chemphys.2011.10.021
61. A. Singh, K.R. Ansari, J. Haque, P. Doharec, H. Lgaz, R. Salghi and M.A. Quraishi, Effect of electron donating functional groups on corrosion inhibition of mild steel in hydrochloric acid: Experimental and quantum chemical study, *J. Taiwan Inst. Chem. Eng*., 2018, **82**, 233–251. doi: 10.1016/j.jtice.2017.09.021
62. Z. Cao, Y. Tang, H. Cang, J. Xu, G. Lu and W. Jing, Novel benzimidazole derivatives as corrosion inhibitors of mild steel in the acidic media. Part II: Theoretical studies, *Corros. Sci*., 2014, **83**, 292–298. doi: 10.1016/j.corsci.2014.02.025
63. T.K. Sarkar, M. Yadav and I.B. Obot, Mechanistic evaluation of adsorption and corrosion inhibition capabilities of novel indoline compounds for oil well/tubing steel in 15% HCl, *Chem. Eng. J*., 2022, **431**, 133481. doi: 10.1016/j.cej.2021.133481
64. M. Belghiti, Y. Karzazi, A. Dafali, I.B. Obot, E.E. Ebenso, K.M. Emran, I. Bahadur, B. Hammouti and F. Bentiss, Anti-corrosive properties of 4-amino-3,5-bis(disubstituted)-1,2,4-triazole derivatives on mild steel corrosion in 2 M H_3PO_4 solution: Experimental and theoretical studies, *J. Mol. Liq*., 2016, **216**, 874–886. doi: 10.1016/j.molliq.2015.12.093
65. A. Singh, K.R. Ansari, M.A. Quraishi, H. Lgaz and Y. Lin, Synthesis and investigation of pyran derivatives as acidizing corrosion inhibitors for N80 steel in hydrochloric acid: theoretical and experimental approaches, *J. Alloy. Compd*., 2018, **762**, 347–362. doi: 10.1016/j.jallcom.2018.05.236

♦ ♦ ♦